

Northumbria Research Link

Citation: Kyriakou, Sotiris, Cheung, William, Mantso, Theodora, Mitsiogianni, Melina, Anestopoulos, Ioannis, Veuger, Stephany, Trafalis, Dimitris T., Franco, Rodrigo, Pappa, Aglaia, Tetard, David and Panayiotidis, Mihalis (2021) A novel methylated analogue of L-Mimosine exerts its therapeutic potency through ROS production and ceramide-induced apoptosis in malignant melanoma. *Investigational New Drugs*, 39 (4). pp. 971-986. ISSN 0167-6997

Published by: Springer

URL: <https://doi.org/10.1007/s10637-021-01087-5> <<https://doi.org/10.1007/s10637-021-01087-5>>

This version was downloaded from Northumbria Research Link: <http://nrl.northumbria.ac.uk/id/eprint/45443/>

Northumbria University has developed Northumbria Research Link (NRL) to enable users to access the University's research output. Copyright © and moral rights for items on NRL are retained by the individual author(s) and/or other copyright owners. Single copies of full items can be reproduced, displayed or performed, and given to third parties in any format or medium for personal research or study, educational, or not-for-profit purposes without prior permission or charge, provided the authors, title and full bibliographic details are given, as well as a hyperlink and/or URL to the original metadata page. The content must not be changed in any way. Full items must not be sold commercially in any format or medium without formal permission of the copyright holder. The full policy is available online: <http://nrl.northumbria.ac.uk/policies.html>

This document may differ from the final, published version of the research and has been made available online in accordance with publisher policies. To read and/or cite from the published version of the research, please visit the publisher's website (a subscription may be required.)

SUPPLEMENTARY MATERIAL

A novel methylated analogue of *L*-Mimosine exerts its therapeutic potency through ROS production and ceramide-induced apoptosis in malignant melanoma

Sotiris Kyriakou^{1,2,3}, William Cheung¹, Theodora Mantso¹, Melina Mitsiogianni¹, Ioannis Anestopoulos^{2,3}, Stephany Veuger¹, Dimitris T. Trafalis⁴, Rodrigo Franco^{5,6}, Aglaia Pappa⁷, David Tetard¹ and Mihalis I. Panayiotidis^{1,2,3*}

¹Department of Applied Sciences, Northumbria University, Newcastle Upon Tyne, UK; ²Department of Cancer Genetics, Therapeutics & Ultrastructural Pathology, The Cyprus Institute of Neurology & Genetics, Nicosia, Cyprus and ³The Cyprus School of Molecular Medicine, The Cyprus Institute of Neurology & Genetics, Nicosia, Cyprus; ⁴Department of Pharmacology, Medical School, National & Kapodistrian University of Athens, Athens, Greece; ⁵Redox Biology Centre and ⁶School of Veterinary Medicine & Biomedical Sciences, University of Nebraska, Lincoln, USA; ⁷Department of Molecular Biology & Genetics, Democritus University of Thrace, Alexandroupolis, Greece

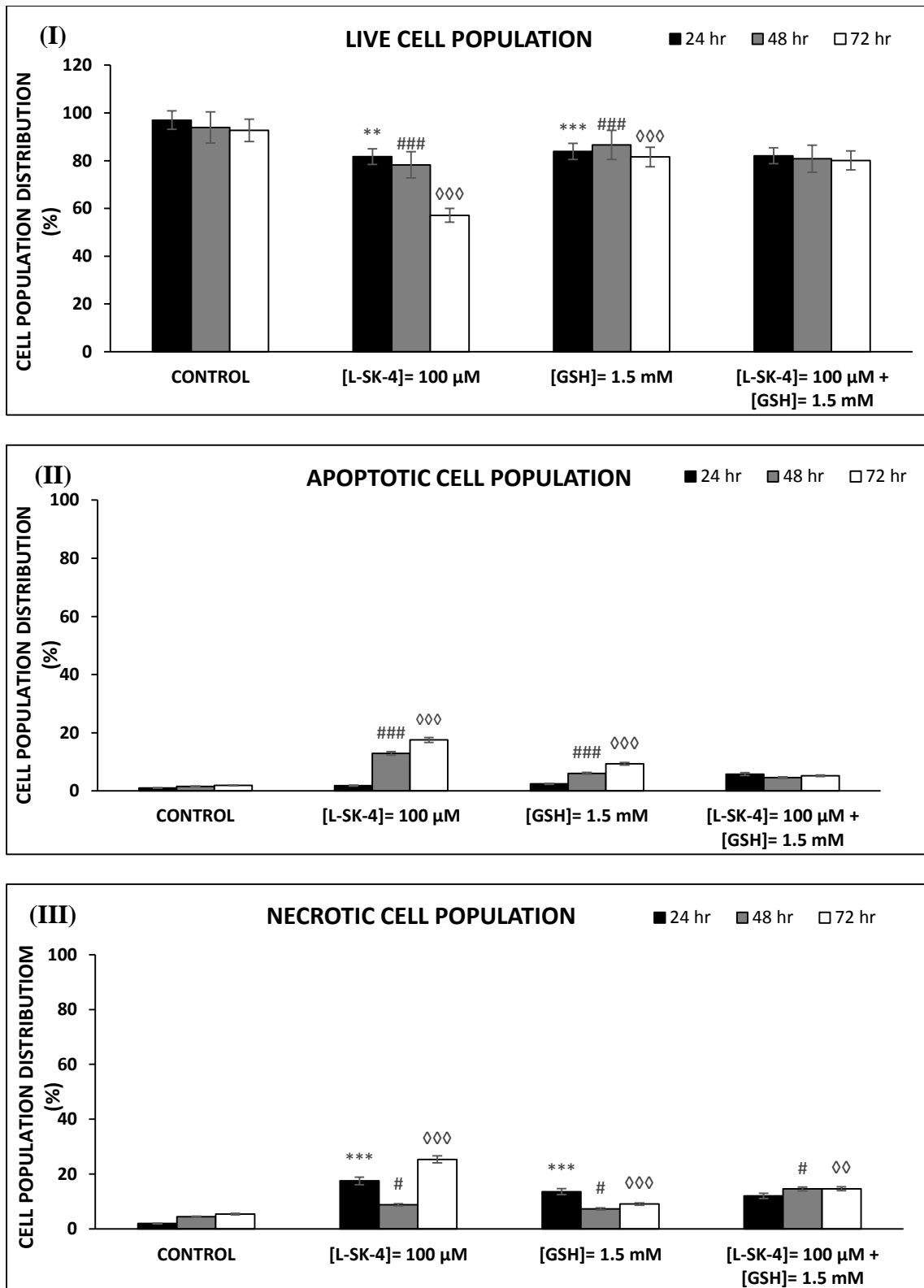


Figure S1: GSH prevents apoptotic induction in VMM-1 cells. Briefly cells were treated with 100 μ M of *L*-SK-4 in the presence or absence of 1.5 mM of GSH for 24, 48 and 72 hrs. A flow cytometry-based approach was utilized for identifying live (I), apoptotic (II) and necrotic (III) cell populations which were quantitated as percentages. Data shown are means of \pm SD of 3 replicates from three independent experiments.

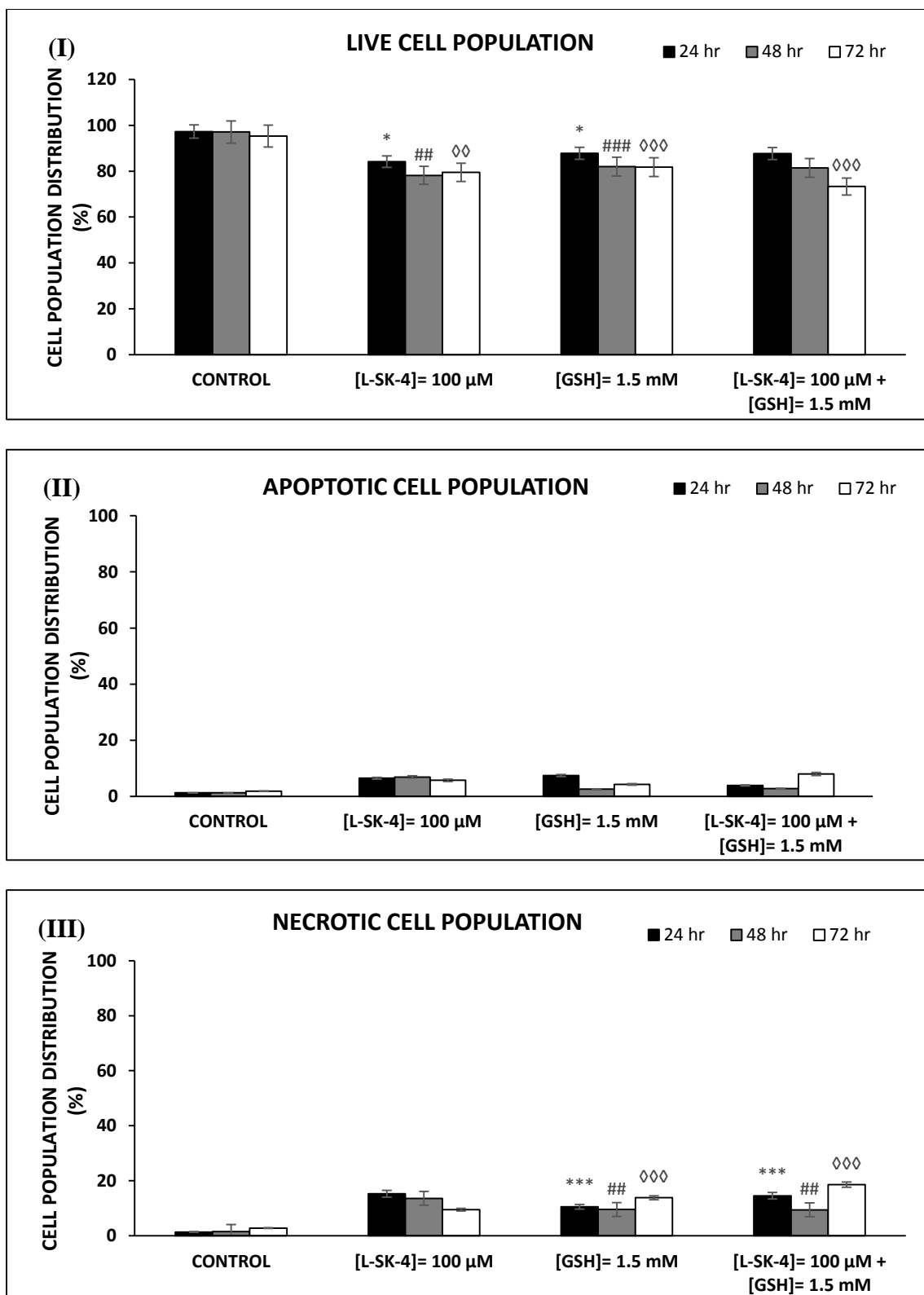


Figure S2. GSH prevents apoptotic induction in Hs 294T cells. Briefly cells were treated with 100 μ M of *L*-SK-4 in the presence or absence of 1.5 mM of GSH for 24, 48 and 72 hrs. A flow cytometry-based approach was utilized for identifying live (I), apoptotic (II) and necrotic (III) cell populations which were quantitated as percentages. Data shown are means of \pm SD of 3 replicates from three independent experiments.

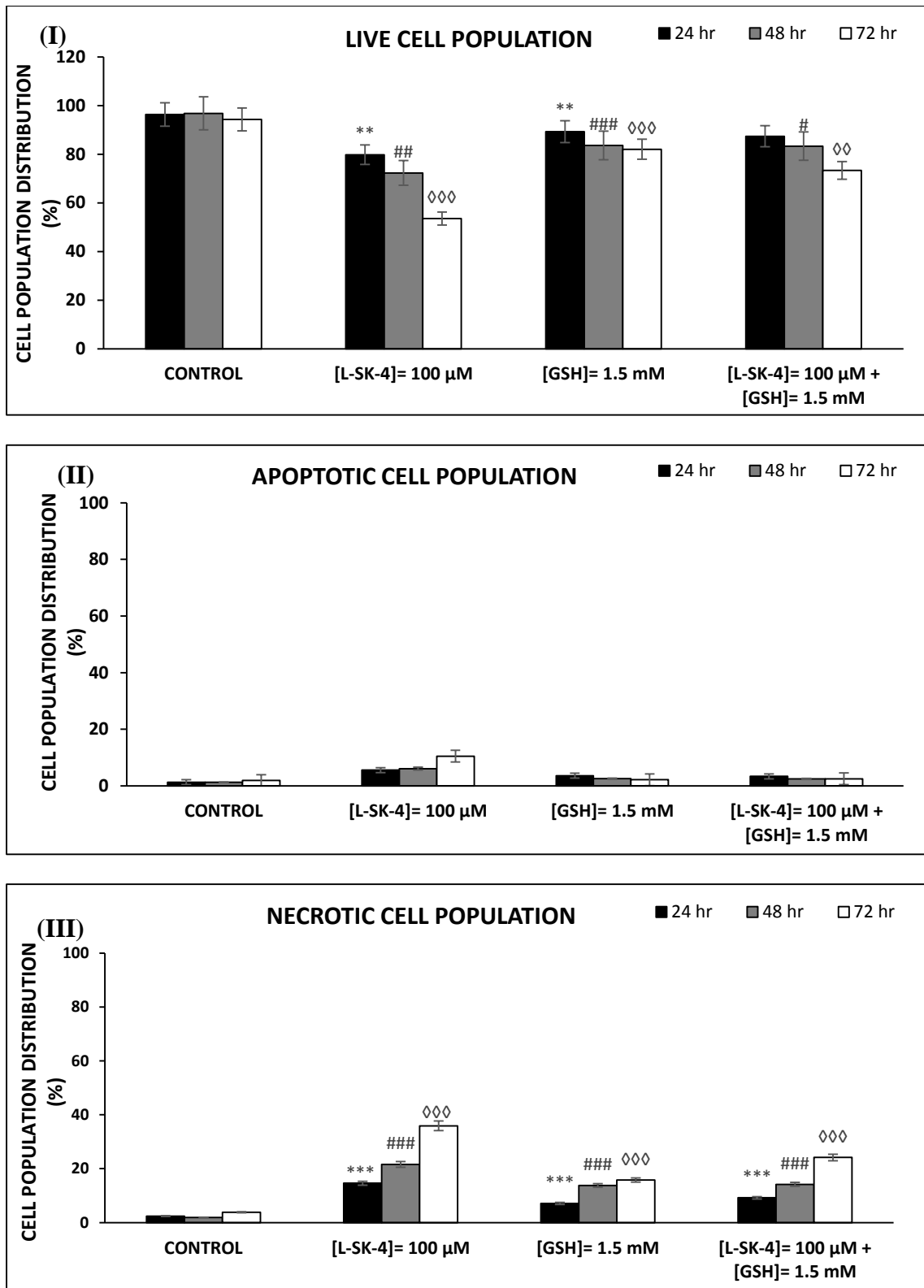


Figure S3. GSH prevents apoptotic and necrotic induction in B16F-10 cells. Briefly cells were treated with 100 μ M of L-SK-4 in the presence or absence of 1.5 mM of GSH for 24, 48 and 72 hrs. A flow cytometry-based approach was utilized for identifying live (I), apoptotic (II) and necrotic (III) cell populations which were quantitated as percentages. Data shown are means of \pm SD of 3 replicates from three independent experiments.

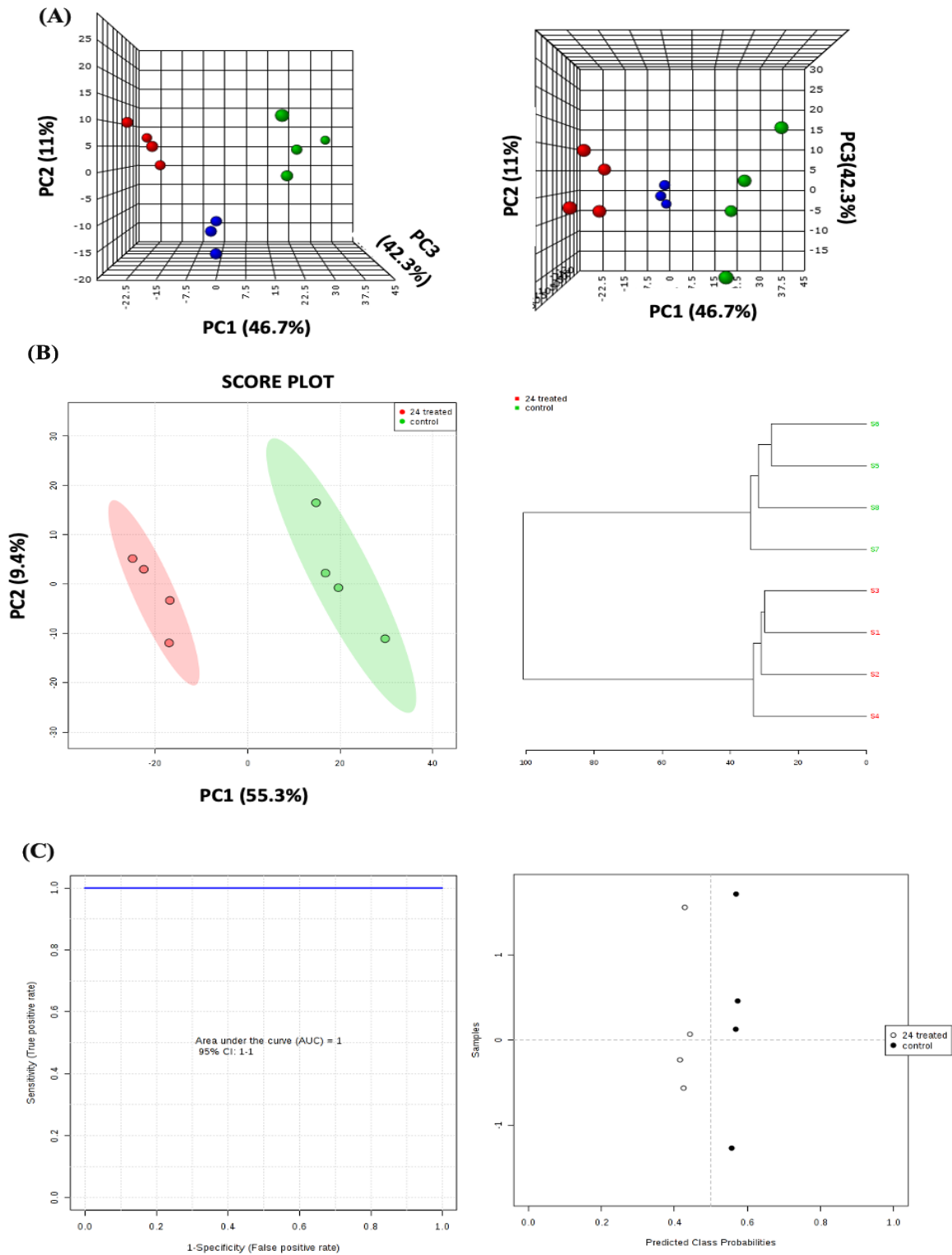


Figure S4: PCA visualization, raw data set approx. 1800 lipid MS features detected (MS1 profiling) n=4. Planar separation can be observed between treated (red spheres), control (green spheres) and quality control (blue spheres) ($x \sim 6\%$ relative standard deviation (r.s.d) –analysis stability assessment). Extraction blank were also imbedded for background ion subtractions prior to PCA visualization. Control and treatment 95% confidence level are highlighted between each groups, approx. 1800 MS features.

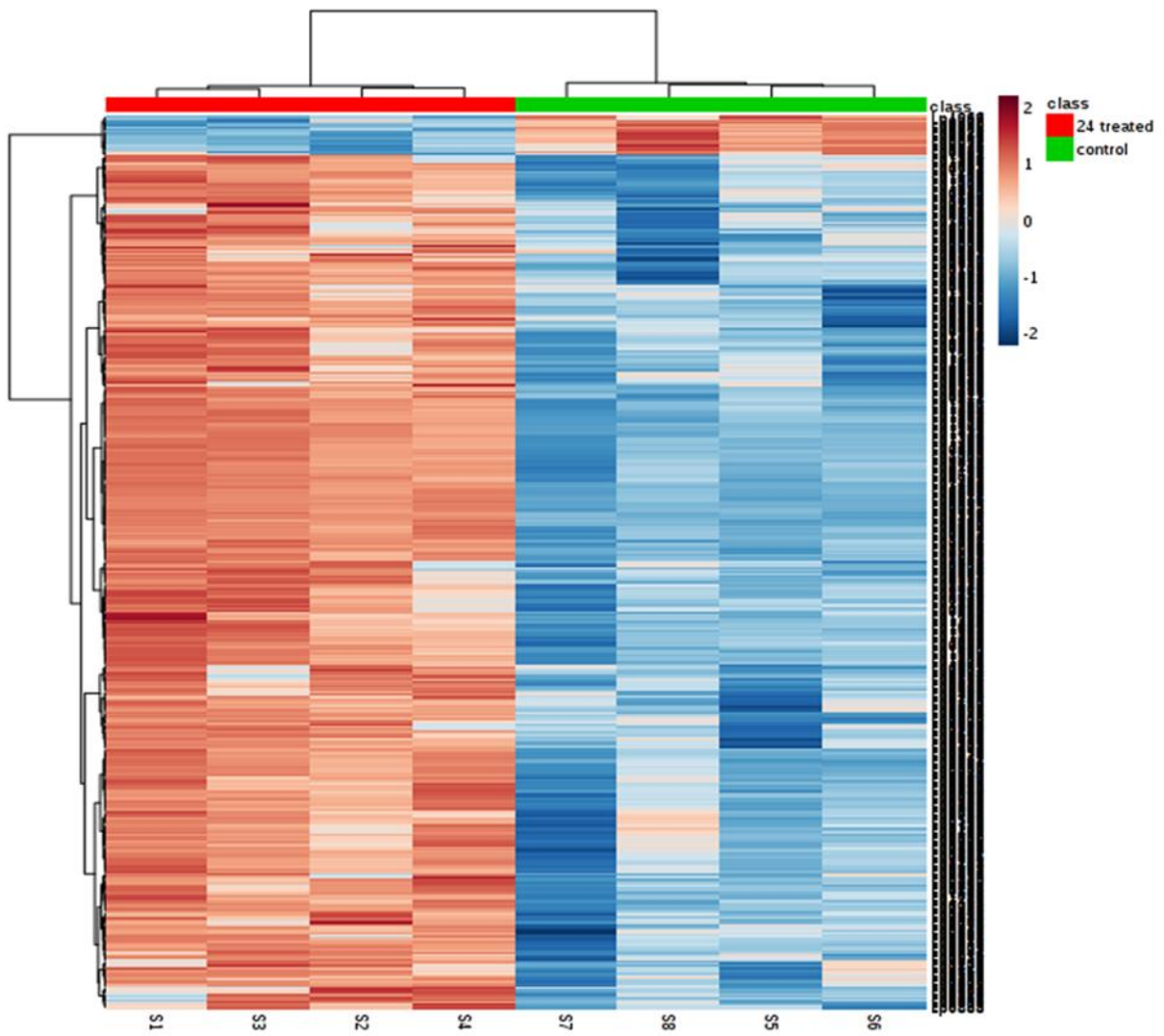


Figure S5: Heat map representation of the top 400 discriminate features, identified via ROC analysis, showing the dysregulation of the lipidome profile of A375 cells exposed to 100 μM *L*-SK-4, for 24 hrs, compared to the respective untreated control.

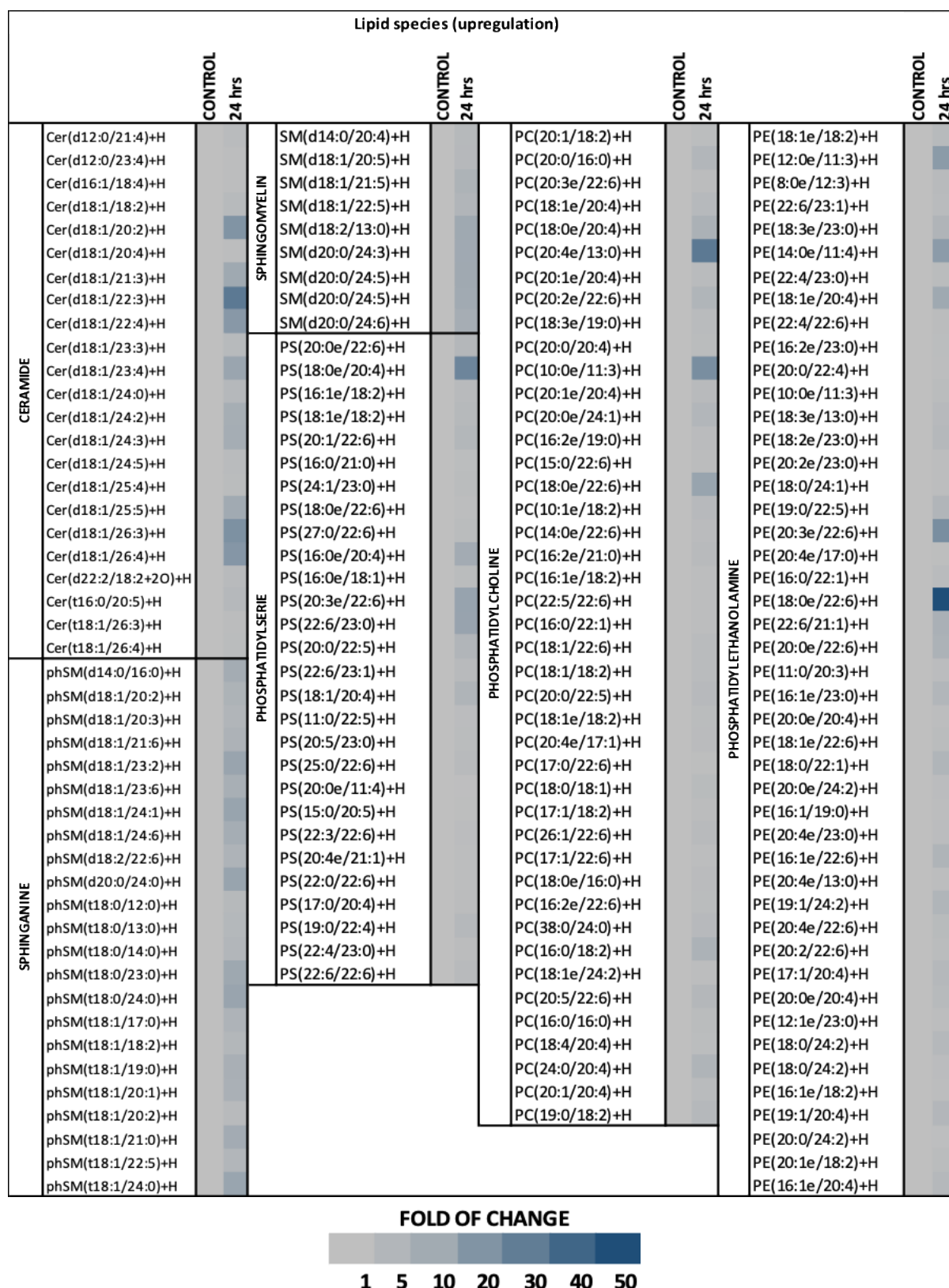


Figure S6: Heat map representation of the sphingolipids' profile of A375 cells between untreated and 24 hrs post treatment with 100 µM *L*-SK-4 experimental conditions.